

Analysis of Unsteady Heat Transfer Problems with Complex Geometries Using Isogeometric Boundary Element Method

Weihoa Fang¹, Zhilin An², Tiantang Yu^{2,*} and Tinh Quoc Bui^{3,4,*}

Abstract: Numerical analysis of unsteady heat transfer problems with complex geometries by the isogeometric boundary element method (IGABEM) is presented. The IGABEM possesses many desirable merits and features, for instance, (a) exactly represented arbitrarily complex geometries, and higher-order continuity due to non-uniform rational B-splines (NURBS) shape functions; (b) using NURBS for both field approximation and geometric description; (c) directly utilizing geometry data from computer-aided design (CAD); and (d) only boundary discretization. The formulation of IGABEM for unsteady heat transfer is derived. The domain discretization in terms of IGABEM for unsteady heat transfer is required as that in traditional BEM. The internal values however are obtained with the analytical formula according to the values on the boundaries, and its computations are therefore mainly dependent on the discretization of the boundaries. The coordinates of internal control points are obtained with the coordinates of control points on the boundaries using Coons body interpolation method. The developed approach is tested with several numerical examples from simple to complicated geometries. Good agreement is gained with reference solutions derived from either analytical or finite element methods.

Keywords: Unsteady heat transfer, BEM, isogeometric analysis, NURBS.

1 Introduction

Heat transfer is one of the important problems that need to be considered in many engineering fields, such as civil engineering, aerospace engineering, mechanical engineering, etc. Temperature change may produce temperature stresses, which consequently affects the safety of structures. For simple geometric shapes with specific boundary conditions, closed-form analytical solutions for the temperature field can be obtained. However, such closed-form analytical approaches are not suitable for problems

¹ Nanjing Automation Institute of Water Conservancy and Hydrology, Nanjing, 210012, China.

² Department of Engineering Mechanics, Hohai University, Nanjing, 211100, China.

³ Institute for Research and Development, Duy Tan University, Da Nang City, Vietnam.

⁴ Department of Civil and Environmental Engineering, Tokyo Institute of Technology, 2-12-1-W8-22, Ookayama, Meguro-ku, Tokyo 152-8552, Japan.

* Corresponding Authors: Tiantang Yu. Email: tiantangyu@hhu.edu.cn;

Tinh Quoc Bui. Email: bui.t.aa@m.titech.ac.jp.

with more complex geometry and boundary conditions. In that circumstance, advanced numerical methods are preferable.

Isogeometric analysis (IGA) uses the NURBS (non-uniform rational B-spline) basis functions in CAD for modeling geometry as shape function in finite element method (FEM) [Hughes, Cottrell and Bazilevs (2005); Shojaee, Valizadeh, Izadpanah et al. (2012)] and references therein. Compared with traditional FEM, IGA owns many desirable features such as exact representation of arbitrarily complex geometries, higher-order continuity and simple mesh refinement. Due to those aforementioned desirable properties, IGA has received extensive attention in recent years, and it gradually becomes a widely used means to solve many engineering problems [Yu, Yin, Bui et al. (2017); Bazilevs, Calo, Zhang et al. (2006); Liu, Yu, Bui et al. (2017); Lai, Yu, Bui et al. (2017); Cottrell, Reali, Bazilevs et al. (2006); Nguyen, Bui, Yu et al. (2014); Lorenzis, Temizer, Wriggers et al. (2011); Fischer, Klassen, Mergheim et al. (2011); Cottrell, Reali, Bazilevs et al. (2006); Wall, Frenzel and Cyron (2008); Seo, Kim and Youn (2010)]. Garcia et al. [Garcia, Bartoň and Pardo (2017); Garcia, Pardo, Dalcin et al. (2017)] proposed a refined isogeometric analysis (rIGA) with the use of highly continuous finite element spaces interconnected with low continuity hyperplanes to maximize the performance of direct solvers, both the solution time and best approximation errors are simultaneously improved. At present, the isogeometric concept is mainly applied to finite element implementation. However, it can also be applied to other methods, and some other hybrid approaches have been recently developed including the extended isogeometric analysis [Yin, Yu, Bui et al. (2016); Yu, Bui, Yin et al. (2016)], isogeometric collocation method [Auricchio, Beirão DA Veiga, Hughes et al. (2017); Manni, Reali and Speleers (2015)], isogeometric meshless method [González, Cueto and Doblaré (2009); Valizadeh, Bazilevs, Chen et al. (2015)], isogeometric boundary element method [Zhou, Liu, Wang et al. (2017)], scaled boundary isogeometric analysis [Natarajan, Wang, Song et al. (2015); Li, Liu and Lin (2017)].

The geometry built by CAD is its boundary curves/surfaces, and the computation of boundary element method (BEM) is mainly performed on the boundary, which means the combination of IGA and BEM is a natural fit, and actually many researches have paid lots of attention on it. Simpson et al. [Simpson, Bordas, Lian et al. (2013); Simpson, Bordas, Trevelyan et al. (2012)] proposed IGABEM for 2-D elastostatic analysis. Subsequently IGABEM has been applied to many other fields such as 3-D potential [Gu, Zhang and Li (2012)], elastostatic problem [Gu, Zhang, Sheng et al. (2011)], shape optimization [Lian, Kerfriden and Bordas (2016); Sun, Yu, Nguyen et al. (2018)], elasto-plastic inclusion problems [Beer, Marussig, Zechner et al. (2016); Bee, Mallardo, Ruocco et al. (2017)], gradient elasticity [Fischer, Klassen, Mergheim et al. (2011)], crack problems [Nguyen, Tran, Anitescu et al. (2016)], and Helmholtz problems [Peake, Trevelyan and Coates (2013); Coox, Atak, Vandepitte et al. (2014)]. Scott et al. [Scott, Simpson, Evans et al. (2013)] coupled IGABEM and T-spline to reduce the number of NURBS patches and improve their smoothness. In order to reduce the computational complexity and computational time, Takahashi and Matsumoto introduced fast multipole method into IGABEM for two-dimensional Laplace equation [Takahashi and Matsumoto (2012)]. Marussig et al. applied fast IGABEM to elasticity [Marussig, Zechner, Beer et al. (2015)], and Campos et al. [Campos, Albuquerque and Wrobel (2017)] applied the

boundary conditions on control points, further improving the applicability of the method. Simpson et al. [Simpson and Liu (2016)] employed a black-box FMM and T-spline to accelerate computation. Beer et al. [Beer, Marussig, Zechner et al. (2014); Wang, Benson and Nagy (2015)] introduced trimmed NURBS technique into IGABEM. Gong et al. [Gong, Dong and Bai (2017)] solved nearly singular integral problems using exponential transformation.

The main objective of the present contribution is to study unsteady heat transfer problems by an effective computational method. In general, the numerical implementation of transient heat transfer is more challenging than that of the steady heat problems. Different from the steady heat transfer [An, Yu, Bui et al. (2018)], the transient heat transfer, which is studied here, has the following features: (1) since the transient temperature problem is time-dependent, the time domain has to be discretized while considering the spatial domain; (2) the differential equation possesses a time derivative term, dealing with the temperature in domain interior is required, i.e., the domain interior is also discretized, while only the boundaries are discretized for the steady heat problem; (3) an exponential integral function is included in the fundamental solution, and special method is required to deal with the computation of the exponential integral function.

Due to the inherent features of NURBS, the boundary and domain of geometry can be represented exactly by data in CAD. This method retains the advantage of mesh refinement on parameter space in IGA. It is important to point out that, for the steady heat transfer using the IGABEM, the discretization is performed only on the boundary, whereas the discretization of domain is still required for unsteady heat transfer as that in traditional BEM. In the IGABEM, the internal values are obtained with the analytical formula according to the values on the boundaries, and the computations mainly focus on the discretized calculations on the boundaries. The coordinates of internal control points are obtained with the coordinates of control points on the boundary using Coons body interpolation method.

The body of this paper is structured as follows. Section 2 briefly presents transient heat transfer problem. In Section 3, the IGABEM formulation for solving transient heat conduction problem is derived in detail. Numerical examples are presented and discussed in Section 4, in which the obtained results are compared with analytical solutions or other methods such as FEM. Some conclusions are drawn in Section 5.

2 Formulation of transient heat transfer analysis

According to the theory of heat transfer, the differential equation of unsteady heat transfer problem in 2-D isotropic solid is given by Yu et al. [Yu, Yao and Gao (2014)]

$$k\nabla^2 T + f = \frac{\partial T}{\partial t} \quad \text{in } \Omega \quad (1a)$$

with

$$k = \frac{\lambda}{c\rho}, \quad f = \frac{w}{c\rho} \quad (1b)$$

where Ω is the domain of geometry, T is the transient temperature, λ the thermal conductivity coefficient, w the heat source, ρ the material density, c the specific heat capacity, t the time, ∇^2 Laplace operator.

The initial condition and the boundary conditions are expressed as follows:

$$T_{t=0} = T_0 \text{ in } \Omega \quad (2a)$$

$$T = \bar{T} \text{ on } \Gamma_1 : \text{Dirichlet boundary} \quad (2b)$$

$$\lambda \frac{\partial T}{\partial \mathbf{n}} = q_2 \text{ on } \Gamma_2 : \text{Neumann boundary} \quad (2c)$$

where T_0 is the initial temperature in the domain; \bar{T} is prescribed temperature, q_2 is prescribed heat flux, while \mathbf{n} is the normal vector pointing outward of boundary.

Using Eqs.(1) and (2), we can obtain the following weighted residual equation:

$$\begin{aligned} & \int_{t_0}^{t_f} \iint_{\Omega} \left(\nabla^2 T + \frac{w}{\lambda} - \frac{1}{k} \frac{\partial T}{\partial t} \right) T^* d\Omega dt + \int_{t_0}^{t_f} \int_{\Gamma_1} (T - \bar{T}) \frac{\partial T^*}{\partial n} d\Gamma dt \\ & - \int_{t_0}^{t_f} \int_{\Gamma_2} \left(\frac{\partial T}{\partial \mathbf{n}} - \frac{q_2}{\lambda} \right) T^* d\Gamma dt = 0 \end{aligned} \quad (3)$$

where T^* is an arbitrary function, t_0 and t_f are two time values.

Integration by parts about Laplace operator item twice, and time derivative item once, and applying the Green formula and boundary conditions, Eq. (3) will be written as [Wu (2008)]

$$\begin{aligned} & \int_{t_0}^{t_f} \iint_{\Omega} \left(\nabla^2 T^* + \frac{1}{k} \frac{\partial T^*}{\partial t} \right) T d\Omega dt + \int_{t_0}^{t_f} \iint_{\Omega} \frac{w}{\lambda} T^* d\Omega dt - \iint_{\Omega} \frac{1}{k} T T^* d\Omega \Big|_{t_0}^{t_f} + \int_{t_0}^{t_f} \int_{\Gamma} T^* \frac{\partial T}{\partial n} d\Gamma dt \\ & - \int_{t_0}^{t_f} \int_{\Gamma} T \frac{\partial T^*}{\partial n} d\Gamma dt = 0 \end{aligned} \quad (4)$$

In this paper, the heat source will not be considered for simplicity, i.e., $w = 0$, so Eq. (4) can be rewritten as

$$\int_{t_0}^{t_f} \iint_{\Omega} \left(\nabla^2 T^* + \frac{1}{k} \frac{\partial T^*}{\partial t} \right) T d\Omega dt - \iint_{\Omega} \frac{1}{k} T T^* d\Omega \Big|_{t_0}^{t_f} + \int_{t_0}^{t_f} \int_{\Gamma} T^* \frac{\partial T}{\partial n} d\Gamma dt - \int_{t_0}^{t_f} \int_{\Gamma} T \frac{\partial T^*}{\partial n} d\Gamma dt = 0 \quad (5)$$

3 IGABEM for unsteady temperature field

3.1 Brief on NURBS basis functions

The knot vector $\mathbf{k}(\xi) = \{\xi_1 = 0, \dots, \xi_i, \dots, \xi_{n+p+1} = 1\}^T$ is defined as a set of non-decreasing numbers that are between zero and one. Here, i is the knot index, ξ_i is the i^{th} knot, n is the number of basis functions, and p is the polynomial order. The NURBS basis function $R_{i,p}(\xi)$ is a weighted average of the B-spline basis functions, is defined as [Hughes, Cottrell and Bazilevs (2005)]

$$R_{i,p}(\xi) = \frac{N_{i,p}(\xi)w_i}{\sum_{k=1}^n N_{k,p}(\xi)w_k} \tag{6}$$

where w_i ($0 < w_i \leq 1$) is the weight, $N_{i,p}(\xi)$ is the i^{th} B-spline basis function of degree p , which is defined recursively as [Hughes, Cottrell and Bazilevs (2005)]

$$N_{i,0}(\xi) = \begin{cases} 1 & \xi_i \leq \xi < \xi_{i+1} \\ 0 & \xi \geq \xi_{i+1} \text{ or } \xi < \xi_i \end{cases} \text{ for } p = 0 \tag{7a}$$

and

$$N_{i,p}(\xi) = \frac{\xi - \xi_i}{\xi_{i+p} - \xi_i} N_{i,p-1}(\xi) + \frac{\xi_{i+p+1} - \xi}{\xi_{i+p+1} - \xi_{i+1}} N_{i+1,p-1}(\xi) \text{ for } p \geq 1 \tag{7b}$$

The two-dimensional NURBS basis functions can be constructed by taking the tensor product of two one-dimensional B-spline basis functions as [Hughes, Cottrell and Bazilevs (2005)]

$$R_{i,j}^{p,q}(\xi, \eta) = \frac{N_{i,p}(\xi)N_{j,q}(\eta)w_{i,j}}{\sum_{i=1}^n \sum_{j=1}^m N_{i,p}(\xi)N_{j,q}(\eta)w_{i,j}} \tag{8}$$

where $w_{i,j}$ are the two-dimensional weights; $N_{i,p}(\xi)$ and $N_{j,q}(\eta)$ are the B-spline basis functions of order p in the ξ direction and order q in the η direction, respectively; $N_{j,q}(\eta)$ follows the recursive formula in Eq. (7) with knot vector $\mathbf{k}(\eta)$. The definition of $\mathbf{k}(\eta)$ is the same as that of $\mathbf{k}(\xi)$.

By using the NURBS basis functions, a NURBS curve of order p can be constructed as

$$\mathbf{x}(\xi) = \sum_{i=0}^n R_{i,p}(\xi) \mathbf{P}_i \tag{9}$$

where \mathbf{P}_i are the coordinates of control point i .

3.2 IGABEM for unsteady temperature field

Taking T^* as the fundamental solution of $k\nabla^2 T + \frac{\partial T}{\partial t} = 0$, yields [Jiang (2008)]

$$k\nabla^2 T^* + \frac{\partial T^*}{\partial t} + \Delta(\mathbf{x}', \mathbf{x})\Delta(t_f, t) = 0 \tag{10}$$

with

$$T^*(\mathbf{x}', \mathbf{x}, t_f, t) = \frac{1}{4\pi k(t_f - t)} e^{-\frac{r^2}{4k(t_f - t)}} \quad (11)$$

where \mathbf{x}' and t_f are regarded as the source point of space and time respectively, \mathbf{x} and t are field point of space and time, $r = \|\mathbf{x} - \mathbf{x}'\|$ is the distance between source point and field point.

Considering $\lim_{t \rightarrow t_f} T^* = \Delta(\mathbf{x}', \mathbf{x})$ and $\lim_{t \rightarrow t_f} \iint_{\Omega} T^* T d\Omega = T(\mathbf{x}', t_f)$, Eq. (5) becomes

$$T(\mathbf{x}', t_f) + k \int_{t_0}^{t_f} \int_{\Gamma} T(\mathbf{x}, t) \frac{\partial T^*(\mathbf{x}', \mathbf{x}, t_f, t)}{\partial n} d\Gamma dt = \quad (12)$$

$$k \int_{t_0}^{t_f} \int_{\Gamma} T^*(\mathbf{x}', \mathbf{x}, t_f, t) \frac{\partial T(\mathbf{x}, t)}{\partial n} d\Gamma dt + \iint_{\Omega} T(\mathbf{x}, t) T^*(\mathbf{x}', \mathbf{x}, t_f, t) d\Omega \Big|_{t_0}$$

with

$$q^* = \frac{\partial T^*(\mathbf{x}', \mathbf{x}, t_f, t)}{\partial n} = -\frac{r}{8\pi k^2 (t_f - t)^2} e^{-\frac{r^2}{4k(t_f - t)}} \frac{\partial r}{\partial n} \quad (13)$$

From Eq. (12), we can find that we can easily get the temperature at points $\mathbf{x}' \in \Omega$ at time t_f when $T(\mathbf{x}, t)$ and $\frac{\partial T(\mathbf{x}, t)}{\partial n}$ are known on all the boundaries. In order to obtain all the unknown temperature and heat flux on the boundary, source point \mathbf{x}' should be placed on the boundary, thus a term $C(\mathbf{x}')$ appears and the boundary integral equation of a point on the boundary is

$$C(\mathbf{x}') T(\mathbf{x}', t_f) + k \int_{t_0}^{t_f} \int_{\Gamma} T(\mathbf{x}, t) \frac{\partial T^*(\mathbf{x}', \mathbf{x}, t_f, t)}{\partial n} d\Gamma dt = \quad (14)$$

$$k \int_{t_0}^{t_f} \int_{\Gamma} T^*(\mathbf{x}', \mathbf{x}, t_f, t) \frac{\partial T(\mathbf{x}, t)}{\partial n} d\Gamma dt + \iint_{\Omega} T(\mathbf{x}, t) T^*(\mathbf{x}', \mathbf{x}, t_f, t) d\Omega \Big|_{t_0}$$

where the term of domain integral represents the influence of initial condition and $C(\mathbf{x}')$ is the same as that in steady heat transfer problem [An, Yu, Bui et al. (2018); Wu (2008)], which is related to the shape of boundary.

$$C(\mathbf{x}') = \begin{cases} 1 & \mathbf{x}' \in \Omega \\ \frac{\beta}{2\pi} & \mathbf{x}' \in \Gamma \text{ (unsmooth boundary points)} \\ \frac{1}{2} & \mathbf{x}' \in \Gamma \text{ (smooth boundary points)} \end{cases} \quad (15)$$

The boundaries are discretized into n non-overlapping elements

$$\Gamma = \sum_{e=1}^{N_e} \Gamma_e, \quad \Gamma_i \cap \Gamma_j = 0, \quad i \neq j \quad (16)$$

The boundary variables are interpolated with shape functions. Time domain is uniformly divided into f steps. In each step ΔT , T and q are considered as be constant, in time step (t_{i-1}, t_i) , Eq. (14) can be rewritten as

$$C(\mathbf{x}')T(\mathbf{x}', t_i) + k \sum_{e=1}^{N_e} \int_{\Gamma_e} \int_{t_{i-1}}^{t_i} q^*(\mathbf{x}', \mathbf{x}, t_f, t) dt \cdot T(\mathbf{x}, t) d\Gamma = \\ k \sum_{e=1}^{N_e} \int_{\Gamma_e} \int_{t_{i-1}}^{t_i} T^*(\mathbf{x}', \mathbf{x}, t_f, t) dt \cdot q(\mathbf{x}, t) d\Gamma + \iint_{\Omega} T(\mathbf{x}, t) T^*(\mathbf{x}', \mathbf{x}, t_f, t) d\Omega \Big|_{t_{i-1}} \quad (17)$$

Integrating T^* and q^* over the time domain, we can get [Wu (2008)]

$$T_i^* = \int_{t_{i-1}}^{t_i} T^*(\mathbf{x}', \mathbf{x}, t_f, t) dt = \frac{1}{4\pi k} E_p(b) \quad (18a)$$

$$q_i^* = \int_{t_{i-1}}^{t_i} q^*(\mathbf{x}', \mathbf{x}, t_f, t) dt = -\frac{1}{2\pi k r} e^{-\frac{r^2}{4k(t_i-t_{i-1})}} \frac{\partial r}{\partial n} \quad (18b)$$

where $E_p(b)$ is an exponential integral function, which can be calculated by the series method, shown as follows:

$$E_p(b) = -c - \ln b + \sum_{a=1}^{\infty} (-1)^{a-1} \frac{b^a}{a \cdot a!} \quad (19a)$$

with

$$b = \frac{r^2}{4k(t_i - t_{i-1})} \quad (19b)$$

where c is the Euler constant.

For $0 \leq b \leq 1$, $E_p(b)$ can be calculated using the first few terms of the series shown in Eq. (19a). In this study, we use the first 10 terms of the series. For $b > 1$, the method of series is not good, and $E_p(b)$ can be calculated with the following formula:

$$E_p(b) = \frac{A}{Bbe^b} \quad (20)$$

with

$$A = b^4 + 8.57332874b^3 + 18.05901697b^2 + 8.6376089b + 0.26777373 \quad (21a)$$

$$B = b^4 + 9.57332234b^3 + 25.63295614b^2 + 21.09965308b + 3.96849692 \quad (21b)$$

Substituting T_i^* and q_i^* into Eq. (17) and changing the integral on physical space to the integral on parent element, yield

$$C(\mathbf{x}')T(\mathbf{x}', t_i) + k \sum_{e=1}^{N_e} \sum_{l=1}^m \int_{-1}^1 q_i^*(\mathbf{x}', \mathbf{x}(\hat{\xi})) N_l^e(\mathbf{x}(\hat{\xi}), t_i) T_l^e J^e(\hat{\xi}) d\hat{\xi} =$$

$$k \sum_{e=1}^{N_e} \sum_{l=1}^m \int_{-1}^1 T_l^*(\mathbf{x}', \mathbf{x}(\hat{\xi})) N_l^e(\mathbf{x}(\hat{\xi}), t_i) q_l^e(\hat{\xi}) J^e(\hat{\xi}) d\hat{\xi} + \iint_{\Omega} T(\mathbf{x}, t) T^*(\mathbf{x}', \mathbf{x}, t_f, t) d\Omega \Big|_{t_i-1} \quad (22)$$

where m is the number of nodes in each element, l is node number, N_l^e is the corresponding local shape function at node l in element e , while T_l^e and q_l^e are temperature and heat flux at node l in element e , $\hat{\xi} \in [-1, 1]$ is local coordinates, $J^e(\hat{\xi})$ is the Jacobian transformation.

NURBS basis function possesses the property of local support [Piegl and Tiller (1997)], so the temperature and heat flux on the boundary can be written as

$$T(\xi, t_i) = \sum_{l=1}^{p+1} R_{l,p}(\xi) T_l^e(t_i) \quad (23a)$$

$$q(\xi, t_i) = \sum_{l=1}^{p+1} R_{l,p}(\xi) q_l^e(t_i) \quad (23b)$$

Substituting Eq. (23) into Eq. (22), yields

$$C(\mathbf{x}') \sum_{l=1}^{p+1} R_{l,p}^e(\hat{\xi}') T_l^{e'}(t_i) + k \sum_{e=1}^{N_e} \sum_{l=1}^{p+1} \left[\int_{-1}^1 q_i^*(\mathbf{x}', \mathbf{x}(\hat{\xi})) R_{l,p}^e(\hat{\xi}) J^e(\hat{\xi}) d\hat{\xi} \right] T_l^e(t_i)$$

$$= k \sum_{e=1}^{N_e} \sum_{l=1}^{p+1} \left[\int_{-1}^1 T_l^*(\mathbf{x}', \mathbf{x}(\hat{\xi})) R_{l,p}^e(\hat{\xi}) J^e(\hat{\xi}) d\hat{\xi} \right] q_l^e(t_i) + \iint_{\Omega} T(\mathbf{x}, t) T^*(\mathbf{x}', \mathbf{x}, t_f, t) d\Omega \Big|_{t_i-1} \quad (24)$$

where $\hat{\xi}'$ is local coordinate of source point, e' the element where source point located in, and the Jacobian of transformation $J^e(\hat{\xi})$ is given by

$$J^e(\hat{\xi}) = \frac{\partial \Gamma}{\partial \xi} \frac{\partial \xi}{\partial \hat{\xi}} = \sqrt{\left(\frac{dx}{d\xi}\right)^2 + \left(\frac{dy}{d\xi}\right)^2} \cdot \frac{\xi_2 - \xi_1}{2} \quad (25)$$

where ξ_1 and ξ_2 are the coordinate of the start and end point of element in parameter space respectively.

In terms of the IGABEM, the nodal points (i.e., control points) may not be situated on the boundary, the collocation points are hence defined as [Johnson (2005)]:

$$\xi'_i = \frac{\xi_{i+1} + \xi_{i+2} + \dots + \xi_{i+p}}{p} \quad i = 1, 2, \dots, n-1 \quad (26)$$

Applying the source point to the discrete nodes, Eq. (24) can be written in matrix form as follows:

$$\mathbf{H}^i \mathbf{T}^i = \mathbf{G}^i \mathbf{q}^i + \mathbf{B}^i \bar{\mathbf{T}}^{i-1} \quad (27)$$

where \mathbf{T}^i is the temperature vector of boundary nodes at time t_i , \mathbf{q}^i the heat flux vector of boundary nodes at time t_i , $\bar{\mathbf{T}}^{i-1}$ the temperature of domain at time t_{i-1} . \mathbf{H}^i , \mathbf{G}^i and \mathbf{B}^i are square matrixes, and their components are the integral of T_i^* , q_i^* on boundary and T^* in domain respectively. Since the time step $\Delta t = t_i - t_{i-1}$ used are spanned equally, \mathbf{H}^i , \mathbf{G}^i and \mathbf{B}^i are the same in each time step, that means \mathbf{H}^i , \mathbf{G}^i and \mathbf{B}^i can be only calculated once, but we need get \mathbf{T}^i and \mathbf{q}^i in each step, and then calculate the temperature of the domain for next step.

The unknown values on the boundary at time t_i can be obtained by solving Eq. (27), and then the temperature of interior points at time t_i can also be calculated by Eq. (14). Thus, there is no need to match the meshes in the domain with the boundary meshes.

3.3 Numerical integration

When the source point is situated in the integral element, strongly singular integral in \mathbf{H}^i and weakly singular integral in \mathbf{G}^i will exist. In general, the singularity subtraction technique (SST) [Guiggiani and Casalini (1987); Yao and Wang (2010)] is used to evaluate strongly singular integral and the transformation approach proposed [Telles (1987)] is used to evaluate weakly singular integral.

There is a domain integral term in boundary integral equation Eq. (24), thus the mesh of domain is inevitable. Using Coons body interpolation method [Long and Zhang (2017)], the coordinates of internal control points can be obtained with the coordinates of control points on the boundary, see the Appendix A. The mesh of domain can be obtained according to the internal control points. In this way, there is a question that how we can get the real temperature at control points of domain. In IGA, the value of control points for computing is a coefficient, not the real temperature. The value of internal control points is the real temperature using Eq. (24). In order to evaluate the domain integral in Eq. (24), it is required that extracting the coordinates of Gaussian integral points for domain integral and their corresponding weights, thus the temperature on the Gaussian integral points at time t_i can be calculated by Eq. (24). The term of domain integral in Eq. (24) can be written as follows:

$$\begin{aligned}
\iint_{\Omega} T(\mathbf{x}, t) T^*(\mathbf{x}', \mathbf{x}, t_f, t) d\Omega \Big|_{t_{i-1}} &= \sum_{e_{in}=1}^{M_e} \sum_{l=1}^{p+1} \sum_{m=1}^{q+1} \int_{-1}^1 \int_{-1}^1 T^* T_{l,m}^{e_{in}}(t_{i-1}) R_{l,m}(\tilde{\xi}, \tilde{\eta}) J^{e_{in}}(\tilde{\xi}, \tilde{\eta}) d\tilde{\xi} d\tilde{\eta} \\
&= \sum_{e_{in}=1}^{M_e} \sum_{gp=1}^{ngp} T^* T_{gp}^{e_{in}}(t_{i-1}) w_{gp} J^{e_{in}}
\end{aligned} \tag{28}$$

where M_e is the number of elements in domain, p and q are the degree in direction and η , l and m are control points number, $T_{l,m}^{e_{in}}(t_{i-1})$ is the temperature of control point at l^{th} in direction ξ and m^{th} in η , in element e_{in} at time t_{i-1} , $R_{l,m}$ is the two-dimensional NURBS basis function calculated by Eq. (8), ngp is the number of Gaussian points in each element, gp is the Gaussian point number, w_{gp} the corresponding weights of Gaussian points, $J^{e_{in}}$ the Jacobian transformation mapping from the parent element to the physical space.

$$J^{e_{in}} = \left| \frac{d\mathbf{x}}{d\tilde{\xi}} \right| = \left| \frac{d\mathbf{x}}{d\xi} \frac{d\xi}{d\tilde{\xi}} \right| \tag{29}$$

It is worth noting that if the boundary condition is a constant, the boundary condition can be directly added to the control points. If the boundary condition is a function distribution, this method cannot work due to its particularities. In IGA, Lagrange multiplier method, penalty method, and Nitsche's method [Nguyen, Kerfriden, Brino et al. (2014); Gu, Yu, Lich et al. (2018)] can be adopted to solve this problem, and the L2 projection method and collocation method are used in IGABEM [Lian, Kerfriden and Bordas (2016)]. Actually, in IGABEM, for the boundary with known boundary condition, we can immediately integrate it by boundary integral equation and only discrete the unknown value of this boundary, thereby avoiding the error caused by applying boundary condition. In the calculation of transient temperature field, BEM does not adopt finite difference approximation for time domain discretization, the integral can be obtained precisely with analytical method by considering the fundamental solution including the time effect in the equation.

3.4 Numerical implementation

Using the above theory and techniques, we summarize the entire process of calculation and show it as follows:

- (1) Read CAD input data including control points, knot vector of both boundary and domain.
- (2) Read material parameter, and determine time step.
- (3) Create boundary elements and domain elements.
- (4) Extract the Gaussian integration points of the domain integral and corresponding weights.
- (5) Create collocation points.

- (6) Set collocation points as source points, loop over collocation points and elements of boundary. (a) If the boundary contains the collocation points, use SST for strong singularity and Tells scheme for weakly singularity. Use Gauss Legendre quadrature for non-singular integral. (b) Generate the global matrices \mathbf{H}^i and \mathbf{G}^i .
- (7) Loop over source points (collocation points), and field points (internal Gaussian integration points), and generate \mathbf{B}^i for calculating unknown values on collocation points.
- (8) Set internal Gaussian points as source points.
- (9) Loop over source points (internal Gaussian points), and field points (also internal Gaussian points), and generate \mathbf{B}^i for calculating unknown values on internal Gaussian points at next time.
- (10) Loop over time.
- (11) Apply boundary conditions.
- (12) Use the temperature of domain at previous time step to calculate the unknown values on boundary at current time step.
- (13) Use the values of the boundary got from Step 12 and the temperature of domain at previous time step to calculate the inner temperature at current time step.

4 Numerical results and discussions

We perform several numerical examples for 2D transient heat transfer problems and discuss their computed results in this section. To show the applicability and effectiveness of the developed IGABEM, examples with both simple and complex geometries are considered. Unless stated otherwise the quadratic order NURBS basis functions are taken for all the implementation. For the numerical integration, 10 Gaussian quadrature points are used for each element, which is determined according to the numerical test.

4.1 A square plate

4.1.1 Zero initial temperature

A square plate with width $a=1$ m as shown in Fig. 1 is considered. The problem conditions are set as follows: the Dirichlet boundary conditions $T=1^\circ C$ on the top side, and $T=0^\circ C$ on the bottom side; the Neumann boundary conditions $q = 0 W/m^2$ on the other sides, and the initial temperature of domain is $T_0=0^\circ C$. $\lambda=1$, $c = 1$, $\rho = 1$, and $k=1$ are used. The analytical solution of these particular geometric and boundary conditions is $T(y,t) = y + \frac{2}{\pi} \sum_{n=1}^{\infty} \frac{\cos(n\pi)}{n} \times \sin(n\pi y) e^{-an^2\pi^2 t}$ [Mansur, Vasconcellos, Zambrozuski et al. (2009)].

The initial knot vector for constructing the geometry of the considered problem is $\mathbf{k}=\{0,0,0,1/4,1/4,1/2,1/2,3/4,3/4,1,1,1\}$ with the weights $\mathbf{w} = \{1,1,1,1,1,1,1,1\}$. Fig. 2 shows the NURBS and control points of boundary, collocation points and element edge,

and NURBS basic functions, and there are 10 elements on each side after refinement. The mesh of domain and related control points are represented in Fig. 3.

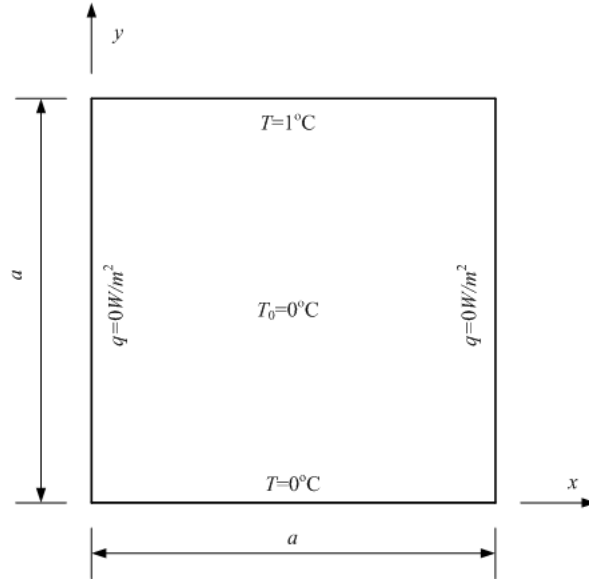
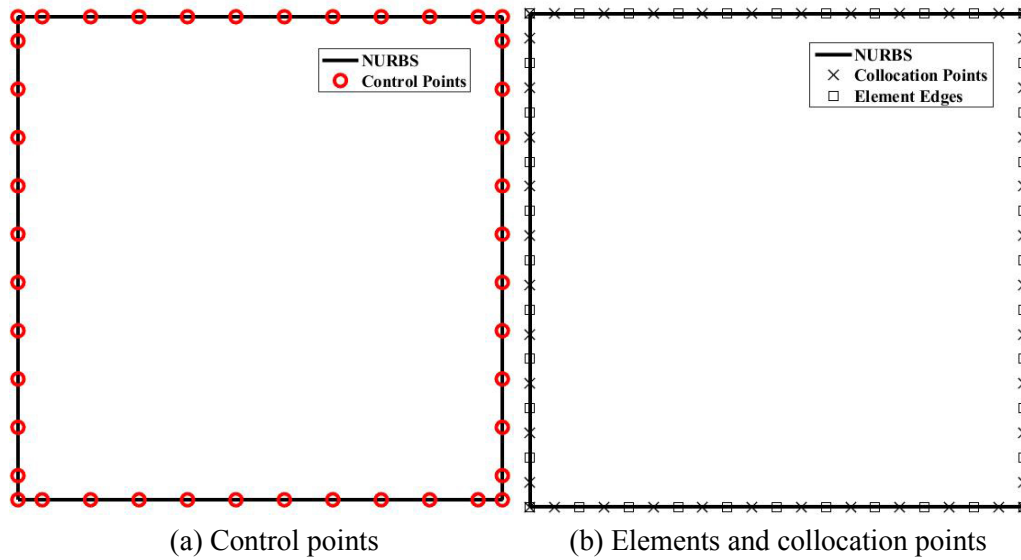
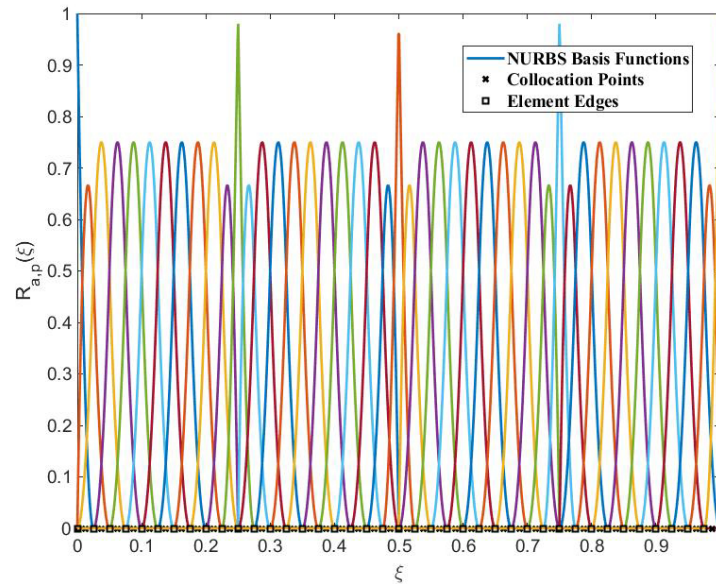


Figure 1: Geometry schematic of a square plate with its Dirichlet and Neumann boundary conditions





(c) NURBS basis functions

Figure 2: Mesh and basis functions

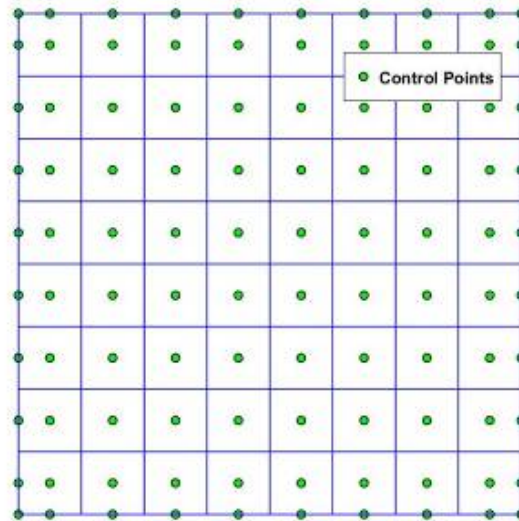


Figure 3: Mesh and control points of domain

Fig. 4 represents the comparison between the obtained numerical results and analytical solution at different time and with different time step of Δt . Interestingly, the developed IGABEM offers acceptable solutions as all the computed results are in good agreement with the exact solutions. It is clear from the results that the smaller the time step Δt is, the higher accuracy is obtained by the IGABEM.

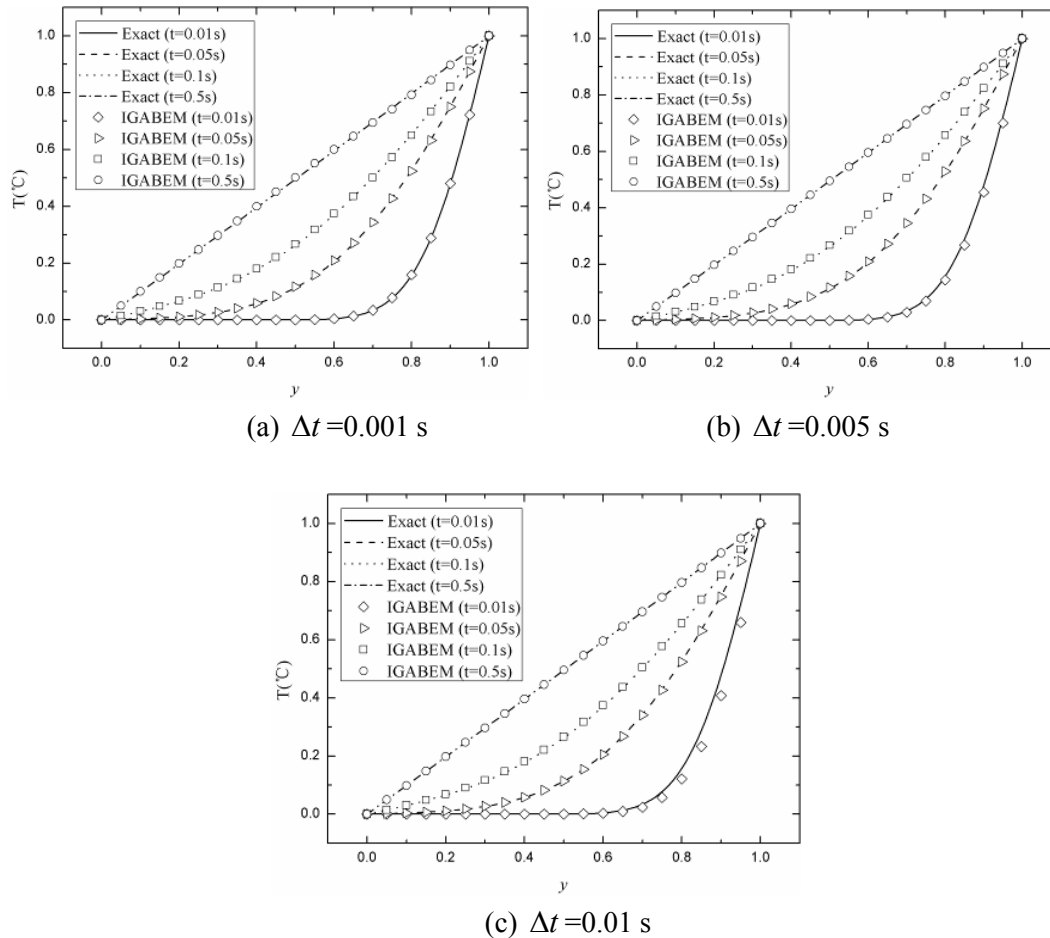


Figure 4: Comparison between the exact solution and IGABEM solutions

Next, the effects of the boundary conditions on the transient response are analyzed. The boundary conditions of the square plate are modified as its change is then shown in Fig. 5. They are, for instance, $T = \sin(\pi x)$ is applied on the top side and $T = 0^\circ\text{C}$ is applied on the other sides. The initial temperature of domain is $T_0 = 0^\circ\text{C}$.

It should be noticed in this example that, since the temperatures at the corners of square are known, but the values of heat conduction are unknown, special corner treatment is required, which is reported in Walker et al. [Walker and Fenner (1989)], and see the Appendix B.

The knot vector, weights and collocation points, elements, control points of boundary, mesh and control points of domain, all of them are the same as those in the above example. The time step $\Delta t = 0.001$ s is used. The distribution of temperature in the domain obtained by the developed IGABEM is compared with that derived from FEM (ANSYS) with 15×15 quadratic elements. As expected, a good agreement between both solutions is obtained.

In the present study, the time step is constant, too large time step may induce large error, while too small time step will lead to inaccurate calculation of exponential integral function. The suitable time step is determined according to the numerical test. When the boundary mesh gets finer, larger time step may be used.

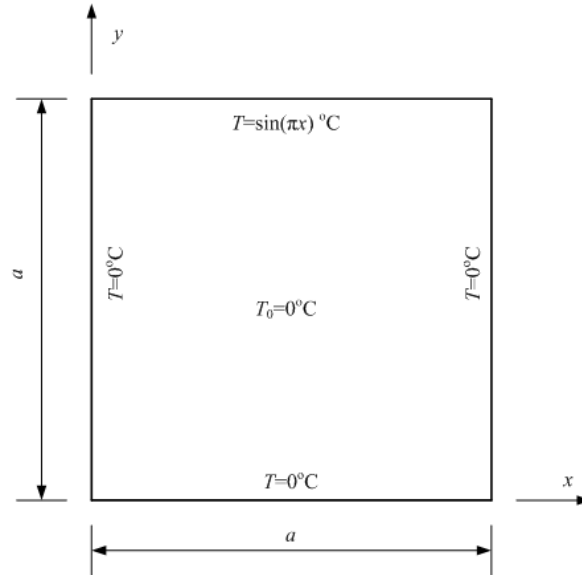
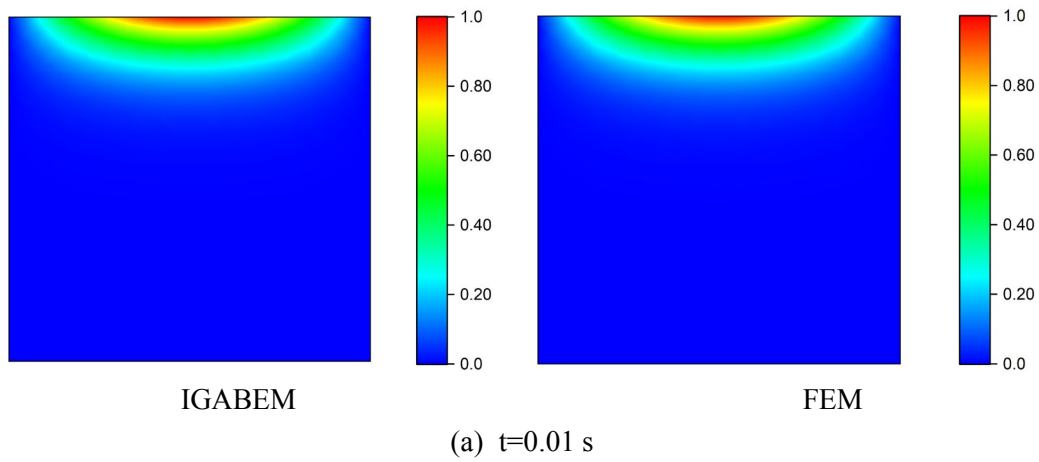


Figure 5: Geometry schematic of a square plate with its Dirichlet boundary conditions



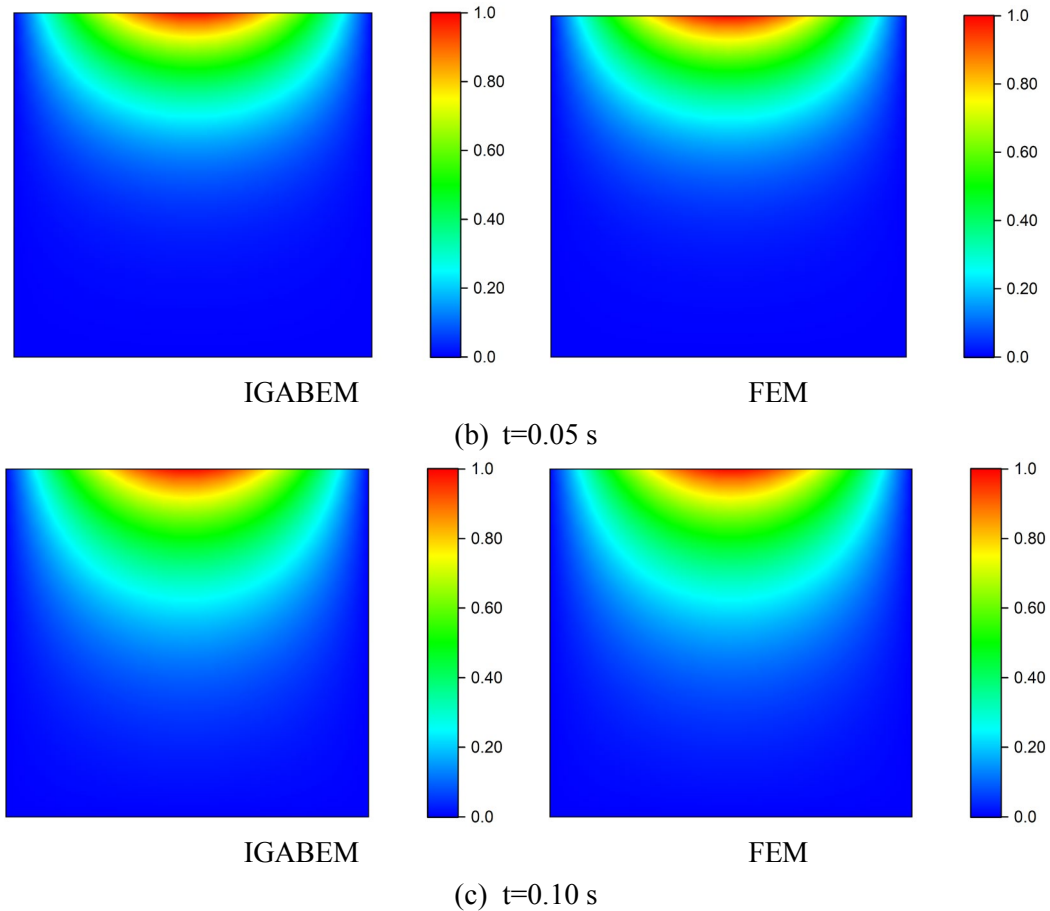


Figure 6: The comparison of the temperature distribution between the developed IGABEM and FEM

4.1.2 Nonzero initial temperature

Consider a square plate with width $a=\pi$ m illustrated in Fig. 7. $T = 0^\circ\text{C}$ is applied on all the boundaries, and different from the previous study, the initial temperature of domain is set to be $T(x, y, 0) = 10 \sin(x) \sin(y)$. The exact solution of this particular problem is available and reported in Nguyen et al. [Nguyen, Bui, Truong et al. (2016)] as $T(x, y, t) = 10 \sin(x) \sin(y) e^{-2t}$, which is used for our comparison purpose.

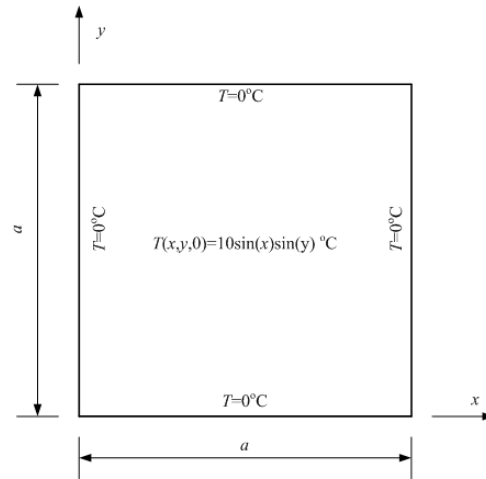


Figure 7: Geometry of square plate and boundary conditions

The number of elements on each side of plate after refinement is 10, the time step $\Delta t = 0.02$ s is taken for this analysis. Two points for instance, $A(0.5\pi, 0.5\pi)$ and $B(0.25\pi, 0.25\pi)$, are selected to be the key points for the analysis, Fig. 8 depicts the temperature of two selected points at different time showing the comparison between the IGABEM results and analytical solution. Not surprisingly, the present method offers remarkable solutions in comparison with the exact formulation. Because the temperatures at all the edges are zero, the temperature at one point in the domain varies from the initial temperature to zero which is the final temperature with increasing the time, e.g., the initial temperatures are 10°C and 5°C at point A and B, respectively, so the temperature at point A and B reduces from 10°C and 5°C to zero with increasing the time, as shown in Fig. 8.

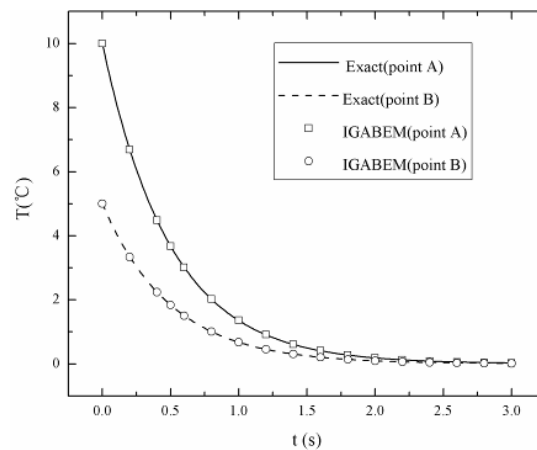


Figure 8: Variation of the temperature of two key points at different time

4.2 A square plate with a circular hole

We now show the applicability of the present approach to solve problems with more complicated geometries. By accomplishing it, we consider a square plate of $0.2 \text{ m} \times 0.2 \text{ m}$ square plate with a circular hole in the center of the plate. The radius of the circular hole is set to be $r=0.05 \text{ m}$. The material parameters are: the conductivity $k=15 \text{ W/m}^\circ\text{C}$, specific heat $c_\rho=125 \text{ J/kg}^\circ\text{C}$ and density $\rho=7800 \text{ kg/m}^3$. $T=200^\circ\text{C}$ is applied on circular hole, and the initial temperature of domain is $T_0=50^\circ\text{C}$. Due to its symmetry, a quarter of the model shown in Fig. 9 is considered and calculated.

The knot vector of initial geometry in this case is $\mathbf{k}=\{0, 0, 0, 1/9, 1/9, 1/3, 1/3, 2/3, 2/3, 7/9, 7/9, 1, 1, 1\}$, the weights are

$\mathbf{w}=\left\{1, 1, 1, \frac{1}{\sqrt{2}}, 1, 1, 1, 1, 1, 1, 1\right\}$. Two points A and B are taken into account for

comparison with the results obtained by ANSYS FEM. Fig. 10 sketches the collocation points, control points and NURBS basis function of initial geometry. The mesh and control points on the boundary and in the domain are shown in Fig. 11. The mesh of 173 quadratic elements in the FEM analysis is depicted in Fig. 12. The computed results of $\Delta t=5 \text{ s}$ are then shown in Fig. 13. In addition, the distribution of temperature at time 200s derived from both the IGABEM and FEM are plotted in Fig. 14, respectively. A good agreement is obtained between the IGABEM result and the FEM result.

As shown in Fig. 13, it is interesting to see that a similar variation of the temperature in the plate at two points A and B is obtained. The developed IGABEM, once again, offers good solutions and all the computed results agree well with the reference FEM solutions.

The temperature at one point in the domain varies from the initial temperature (50°C) to the specified final temperature (200°C) with increasing the time. Because the distance is different between one point and the hole boundary, the temperature at one point is hence different at one time. The temperature in the area closer to the face (boundary) with the highest temperature will approach faster to the maximum temperature than those areas that are far from the particular boundary, e.g., the location of Point A to the hole boundary is closer than that of Point B, so the temperature at Point A is bigger than that of Point B until the same temperature is achieved at last, as shown in Fig. 13.

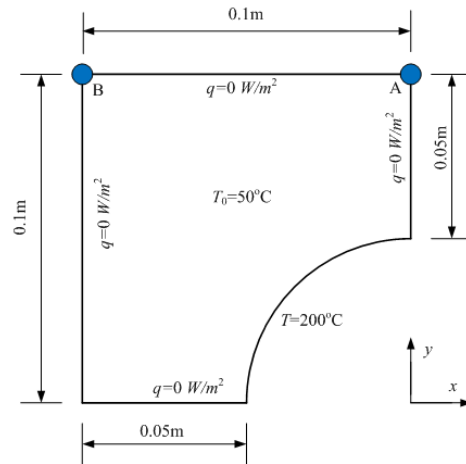
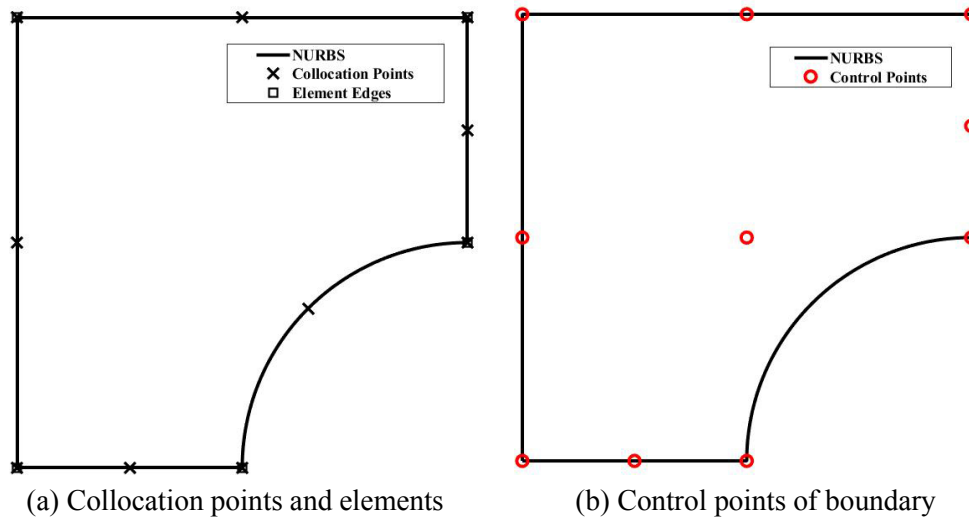
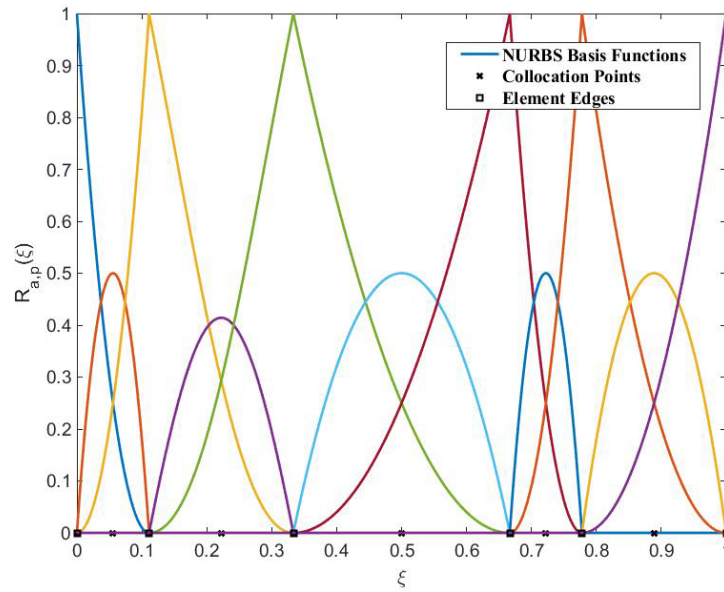


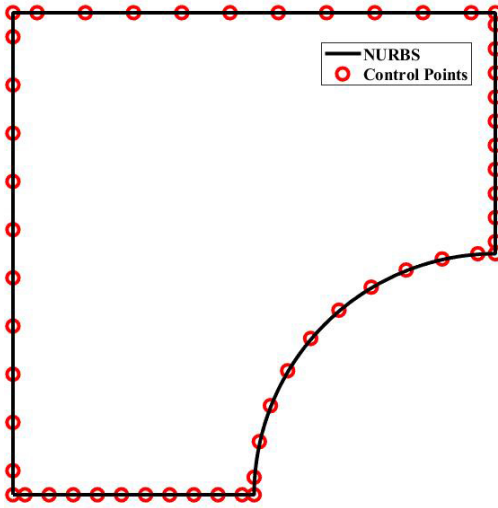
Figure 9: A quarter of geometry



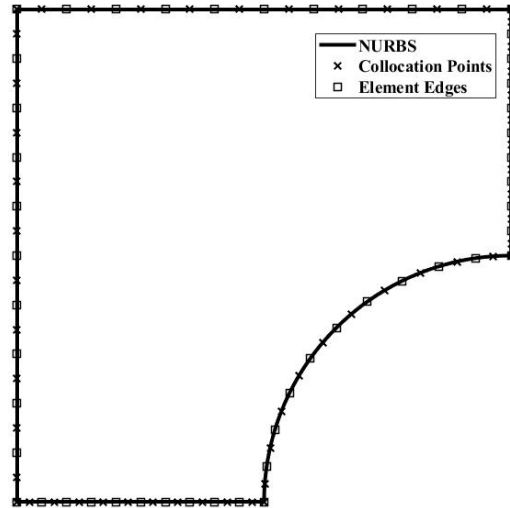


(c) NURBS basis functions

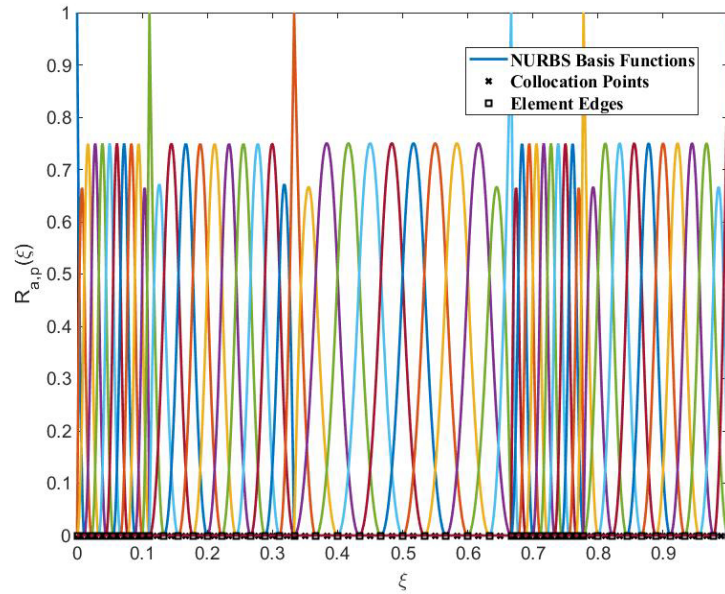
Figure 10: Mesh and basis functions



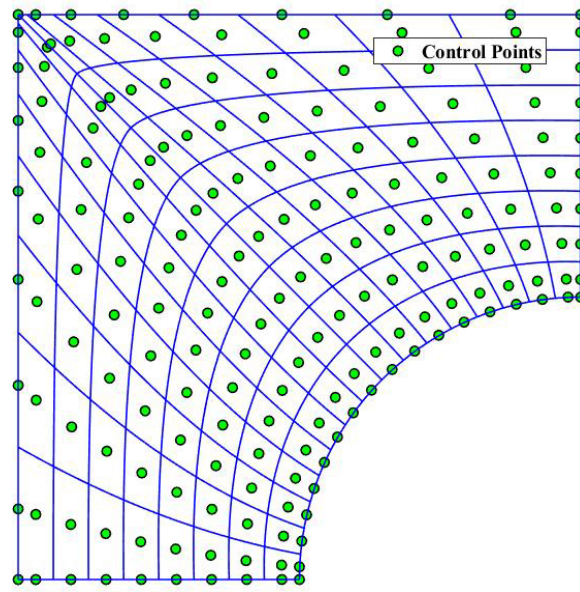
(a) Control points



(b) Mesh and collocation points



(c) NURBS basis functions



(d) Mesh and control points of domain

Figure 11: Mesh and control points after refinement

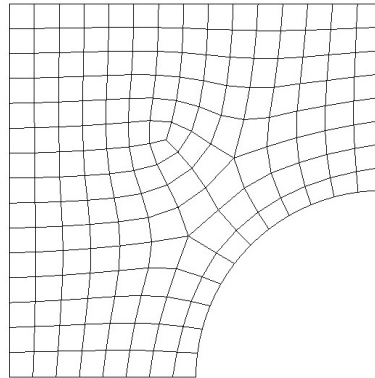


Figure 12: The FEM mesh

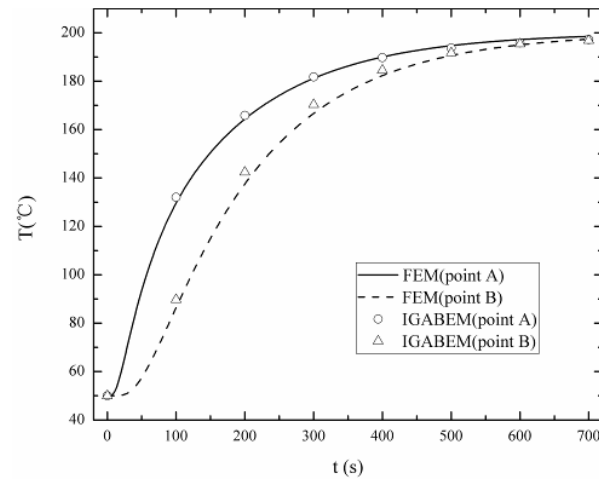
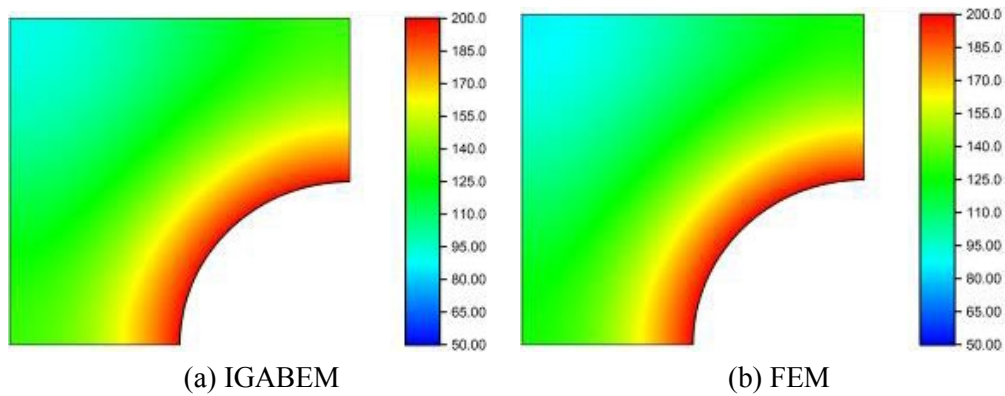


Figure 13: Comparison of temperature variation between the IGABEM and FEM



(a) IGABEM

(b) FEM

Figure 14: Distribution of temperature at time 100 s

4.3 Heat convection in a complex domain

In the last example, the problem of multi-boundary with complicated geometry is considered. The geometry and boundary condition of considered structure are shown in Fig. 15, in which the unmarked boundaries are regarded as adiabatic boundaries. The properties of material are as follows: thermal conductivity is $391 \text{ W/m}^\circ\text{C}$, density is 8940 kg/m^3 , and specific heat is $385.2 \text{ J/kg}^\circ\text{C}$. The outer boundary and the inner boundary are built respectively, and it is noted that the outer boundary is constructed in a counterclockwise way, different from the inner boundary which is built in a clockwise way. Fig. 16 represents the control points, collocation points and NURBS basis function of the initial geometric boundaries. The Gaussian integration points for domain integral are extracted by IGA, and the initial elements and control points of domain are shown in Fig. 17.

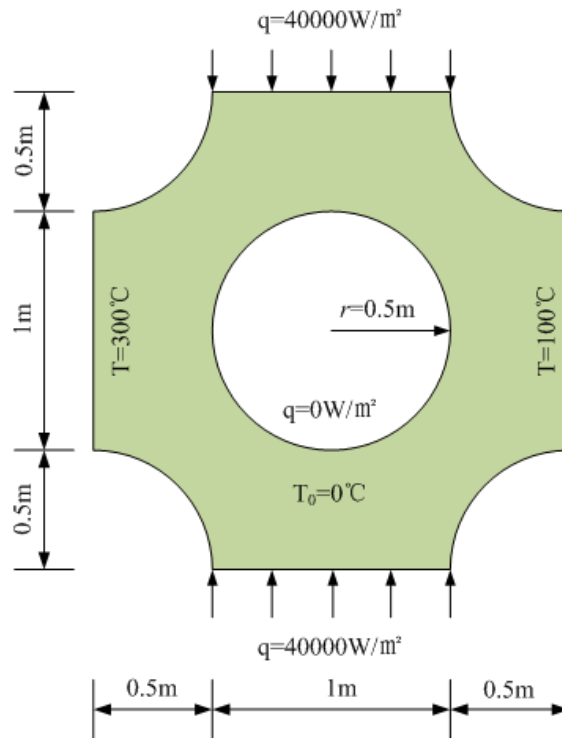
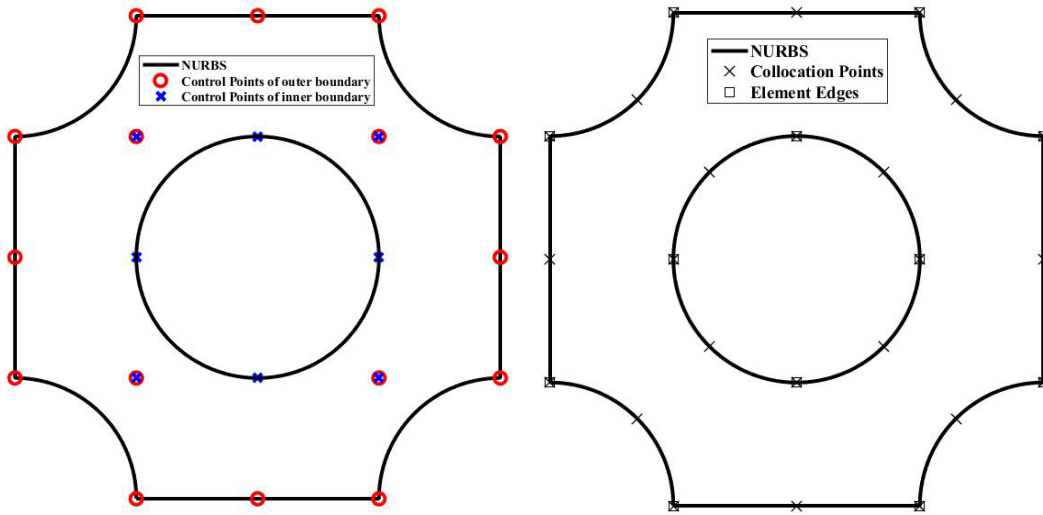
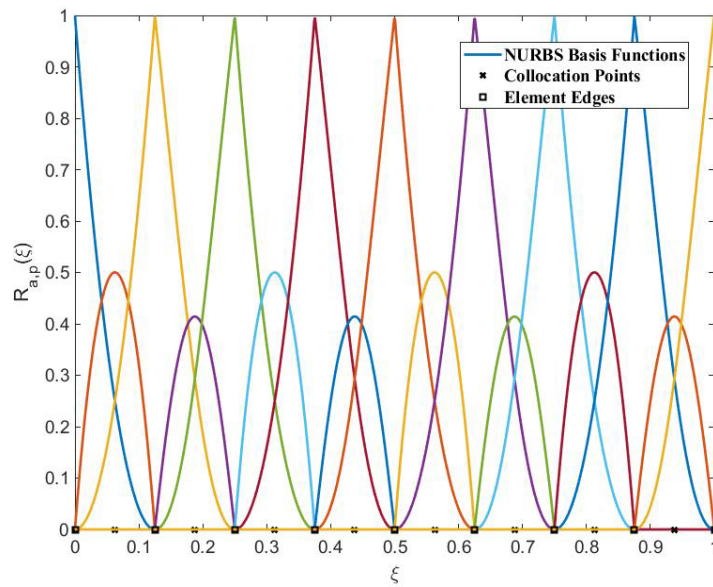


Figure 15: Geometry and boundary conditions

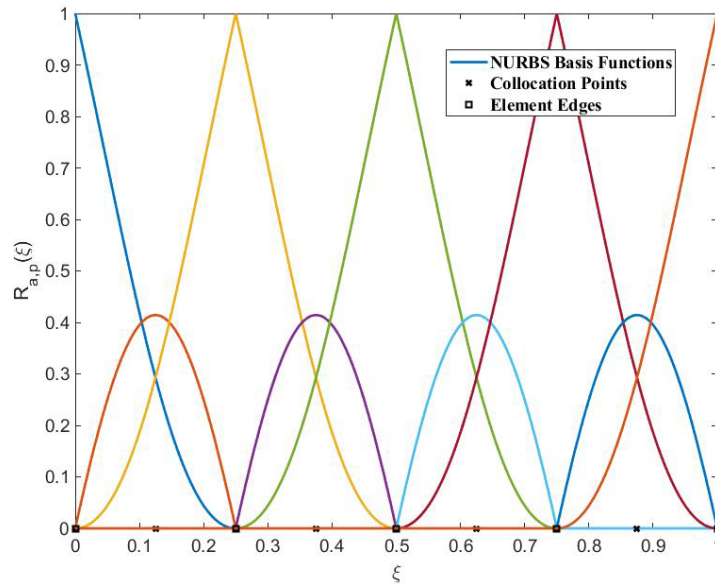


(a) Control points of boundary

(b) Collocation points and element



(c) NURBS basis function of outer boundary



(d) NURBS basis function of inner boundary

Figure 16: Control points and basis function of the boundary

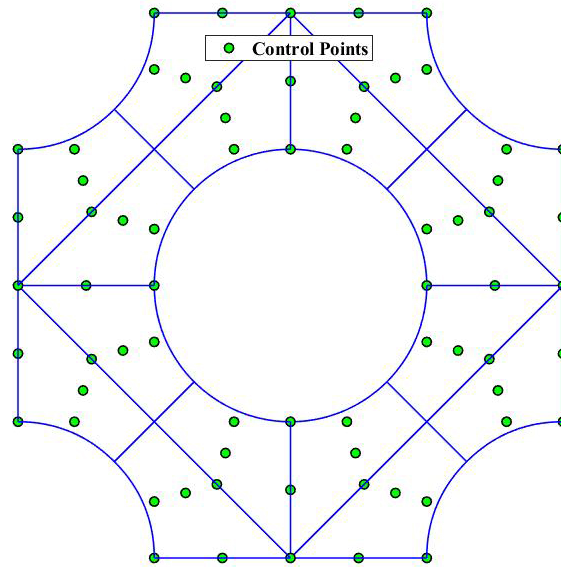


Figure 17: Control points and mesh of domain

In order to enhance the accuracy of the solution, or a better result, the original elements are refined into 10 new elements, which are shown in Fig. 18. In this problem, the time step is $\Delta t = 500$ s. Also, Fig. 19 shows the mesh of FEM (1228 quadratic elements). The temperature distributions estimated at different time by the present IGABEM are compared

with the result computed by ANSYS FEM. The comparison results are hence plotted in Fig. 20. As expected, the IGABEM results match well with the FEM reference solutions.

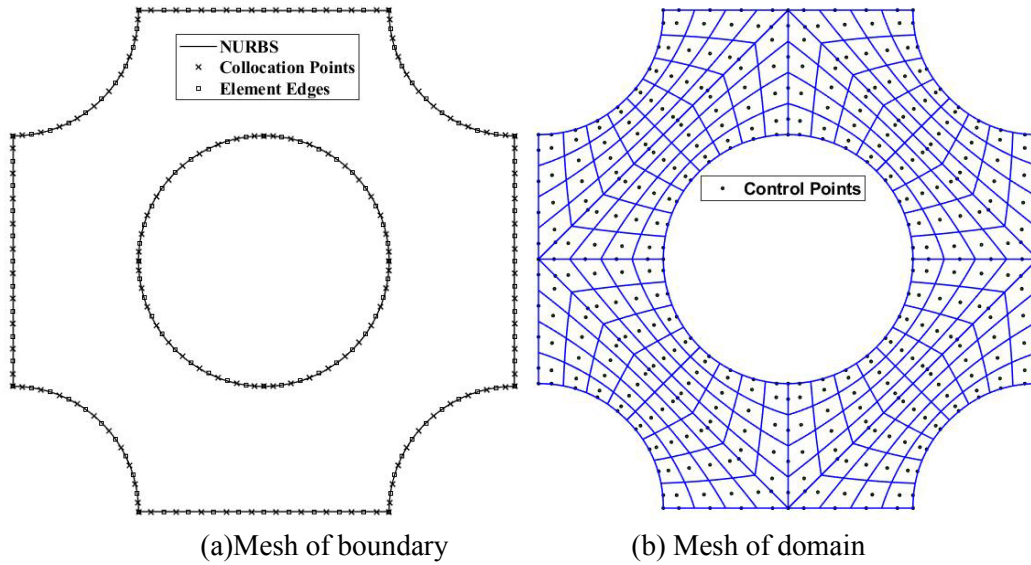


Figure 18: The refined mesh and collocation points

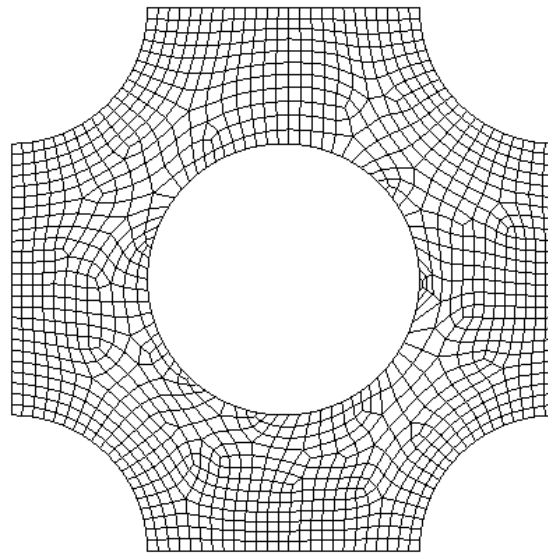


Figure 19: Mesh of FEM

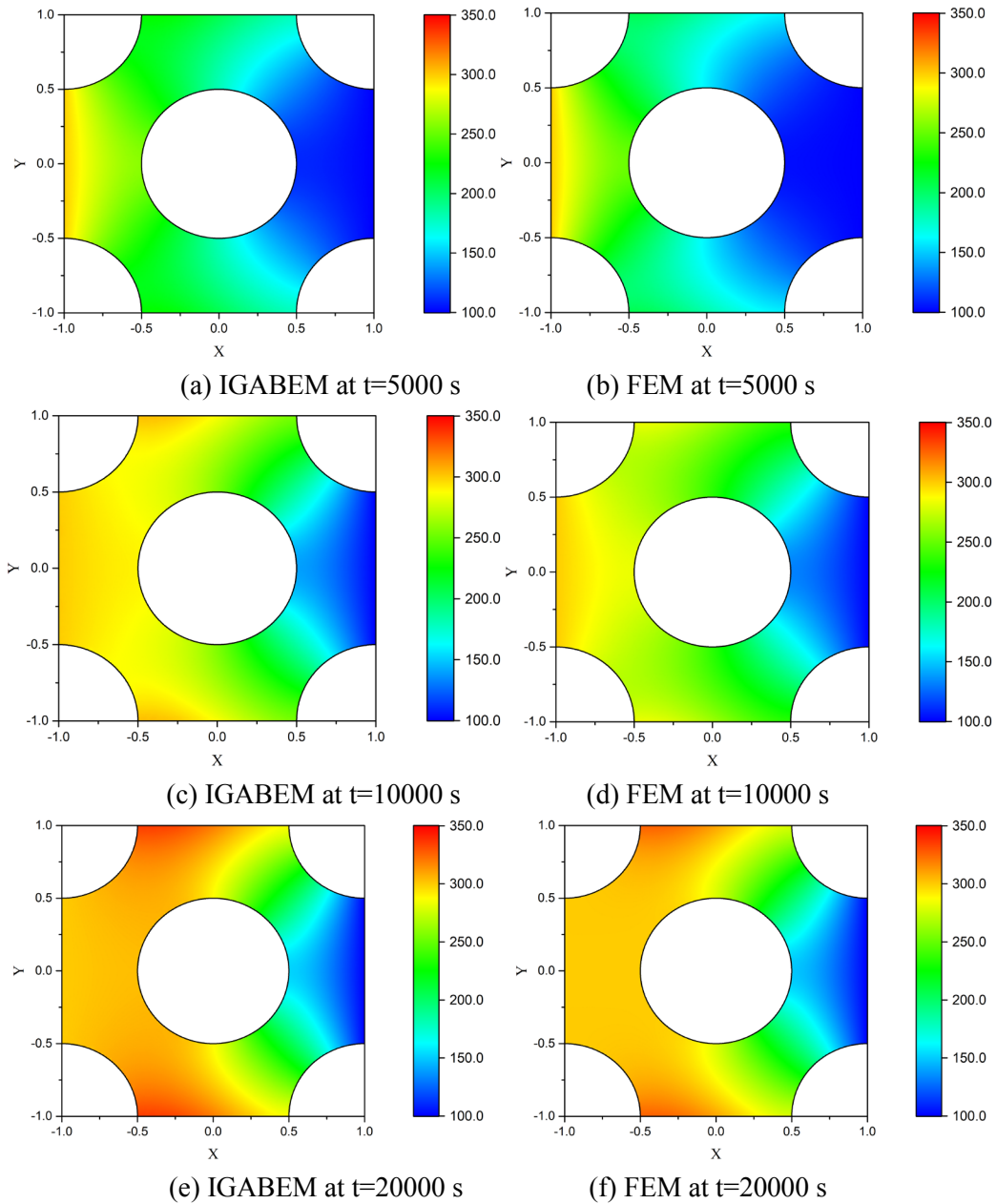


Figure 20: Comparison of the distribution of temperature at different time between the IGABEM and ANSYS FEM

5 Conclusion and outlook

In this paper, two-dimensional unsteady heat transfer problems have been solved with the IGABEM, in which the NURBS basis functions are used to approximate the geometry

and temperature fields. Arbitrarily complex geometries can be exactly represented and higher-order continuity is obtained. In IGABEM, the discretization of domain is required for unsteady heat transfer problem. This is different from the steady heat transfer problem, in which the discretization of domain is avoided. However, the internal values are obtained with the analytical formula according to the values on the boundaries, so the computations mainly focus on the discretized calculations on the boundaries. Through numerical examples, the obtained results and validated results with reference solutions show good performance and high accuracy of the proposed method. One interesting problem that left behind this contribution would be prefer to 3-D cases, which however has been scheduled for our future works.

NURBS-based IGA only works well for quadrilateral domains. For the complex domain problems, there are two ways to deal with them to some extent, i.e., subdividing the design domain of complex topology into multiple quadrilateral patches [Manh, Evgrafov, Gersborg et al. (2011); Qian and Sigmund (2011)] and using trimmed surfaces [Seo, Kim, and Youn (2010)]. How to automatically construct NURBS parameterization of a complex design domain remains an open issue.

Acknowledgement: This work was supported by Natural Science Foundation of Jiangsu Province of China (BK20151070). The financial supports are gratefully acknowledged.

Conflicts of Interest: The authors declare that they have no conflicts of interest to report regarding the present study.

References

- An, Z. L.; Yu, T. T.; Bui, T. Q.; Wang, C.; Trinh, N. A.** (2018): Implementation of isogeometric boundary element method for 2-D steady heat transfer analysis. *Advances in Engineering Software*, vol. 116, pp. 36-49.
- Auricchio, F.; Beirão, D. A.; Veiga, L.; Hughes, T. J. R.; Reali, A. et al.** (2017): Isogeometric collocation methods. *Mathematical Models and Methods in Applied Sciences*, vol. 20, no. 11, pp. 2075-2107.
- Bazilevs, Y.; Calo, V. M.; Zhang, Y.; Hughes, T. J. R.** (2006): Isogeometric fluid-structure interaction analysis with applications to arterial blood flow. *Computational Mechanics*, vol. 38, no. 4-5, pp. 310-322.
- Bee, G.; Mallardo, V.; Ruocco, E.; Marussig, B.; Zechner, J. et al.** (2017): Isogeometric Boundary Element analysis with elasto-plastic inclusions. Part 2: 3-D problems. *Computer Methods in Applied Mechanics and Engineering*, vol. 315, pp. 418-433.
- Beer, G.; Marussig, B.; Zechner, J.; Dünser, C.; Fries, T. P.** (2014): Boundary Element Analysis with trimmed NURBS and a generalized IGA approach. *Eprint Arxiv*, vol. 1, pp. 282-291.
- Beer, G.; Marussig, B.; Zechner, J.; Dünser, C.; Fries, T. P.** (2016): Isogeometric boundary element analysis with elasto-plastic inclusions. Part 1: plane problems. *Computer Methods in Applied Mechanics and Engineering*, vol. 308, pp. 552-570.

- Campos, L. S.; Albuquerque, E. L.; Wrobel, L. C.** (2017): An ACA accelerated isogeometric boundary element analysis of potential problems with non-uniform boundary conditions. *Engineering Analysis with Boundary Elements*, vol. 80, pp. 108-115.
- Coox, L.; Atak, O.; Vandepitte, D.; Desmet, W.** (2014): An isogeometric indirect boundary element method for Helmholtz problems. *Conference on Noise and Vibration Engineering*.
- Cottrell, J. A.; Reali, A.; Bazilevs, Y.; Hughes, T. J. R.** (2006): Isogeometric analysis of structural vibrations. *Computer Methods in Applied Mechanics and Engineering*, vol. 195, no. 41, pp. 5257-5296.
- Fischer, P.; Klassen, M.; Mergheim, J.; Steinmann, P.** (2011): Isogeometric analysis of 2D gradient elasticity. *Computational Mechanics*, vol. 47, no. 3, pp. 325-334.
- Fischer, P.; Klassen, M.; Mergheim, J.; Steinmann, P.; Müller, R.** (2011): Isogeometric analysis of 2D gradient elasticity. *Computational Mechanics*, vol. 47, no. 3, pp. 325-334.
- Garcia, D.; Bartoň, M.; Pardo, D.** (2017): Optimally refined isogeometric analysis. *Procedia Computer Science*, vol. 108, pp. 808-817.
- Garcia, D.; Pardo, D.; Dalcin, L.; Paszyński, M.; Collier, N. et al.** (2017): The value of continuity: refined isogeometric analysis and fast direct solvers. *Computer Methods in Applied Mechanics and Engineering*, vol. 316, pp. 586-605.
- Gong, Y. P.; Dong, C. Y.; Bai, Y.** (2017): Evaluation of nearly singular integrals in isogeometric boundary element method. *Engineering Analysis with Boundary Elements*, vol. 75, pp. 21-35.
- González, D.; Cueto, E.; Doblaré, M.** (2009): Towards an isogeometric meshless natural element method. *Progress on Meshless Methods*, pp. 237-257.
- Gu, J.; Yu, T.; Lich, L. V.; Nguyen, T. T.; Bui, T. Q.** (2018): Adaptive multi-patch isogeometric analysis based on locally refined B-splines. *Computer Methods in Applied Mechanics and Engineering*, vol. 339, pp. 704-738.
- Gu, J.; Zhang, J.; Li, G.** (2012): Isogeometric analysis in BIE for 3-D potential problem. *Engineering Analysis with Boundary Elements*, vol. 36, no. 5, pp. 858-865.
- Gu, J.; Zhang, J.; Sheng, X.; Li, G.** (2011): B-spline approximation in boundary face method for three-dimensional linear elasticity. *Engineering Analysis with Boundary Elements*, vol. 35, no. 11, pp. 1159-1167.
- Guiggiani, M.; Casalini, P.** (1987): Direct computation of Cauchy principal value integrals in advanced boundary element. *International Journal for Numerical Methods in Engineering*, vol. 24, no. 9, pp. 1711-1720.
- Hughes, T. J. R.; Cottrell, J. A.; Bazilevs, Y.** (2005): Isogeometric analysis: CAD, finite elements, NURBS, exact geometry and mesh refinement. *Computer Methods in Applied Mechanics and Engineering*, vol. 194, no. 39-41, pp. 4135-4195.
- Jiang, H. D.** (2008): *The Boundary Element Method for Elasticity Problem*. China Water & Power Press, Beijing.

Johnson, R. (2005): Higher order B-spline collocation at the Greville abscissa. *Applied Numerical Mathematics*, vol. 52, pp. 63-75.

Lai, W. J.; Yu, T. T.; Bui, T. Q.; Wang, Z.; Curiel-Sosa, J. L. et al. (2017): 3-D elasto-plastic large deformations: IGA simulation by Bezier extraction of NURBS. *Advances in Engineering Software*, vol. 168, pp. 68-82.

Li, P.; Liu, J.; Lin, G. (2017): A NURBS-based scaled boundary finite element method for the analysis of heat conduction problems with heat fluxes and temperatures on side-faces. *International Journal of Heat and Mass Transfer*, vol. 113, pp. 764-779.

Lian, H.; Kerfriden, P.; Bordas, S. P. A. (2016): Implementation of regularized isogeometric boundary element methods for gradient-based shape optimization in two-dimensional linear elasticity. *International Journal for Numerical Methods in Engineering*, vol. 106, no. 12, pp. 972-1017.

Liu, S.; Yu, T. T.; Bui, T. Q.; Yin, S. H.; Thai, D. K. et al. (2017): Analysis of functionally graded plates by a simple locking-free quasi-3D hyperbolic plate isogeometric method. *Composites Part B: Engineering*, vol. 120, pp. 182-196.

Long, C.; Zhang, G. (2017): Three dimensional structural shape optimization based on sensitivity analysis using isogeometric analysis. *China Mechanical Engineering*, vol. 28, no. 14, pp. 1723-1729.

Lorenzis, L. D.; Temizer, I.; Wriggers, P.; Zavarise, G. (2011): A large deformation frictional contact formulation using NURBS-based isogeometric analysis. *International Journal for Numerical Methods in Engineering*, vol. 87, no. 13, pp. 1278-1300.

Manh, N. D.; Evgrafov, A.; Gersborg, A. R.; Gravesen, J. (2011): Isogeometric shape optimization of vibrating membranes. *Computer Methods in Applied Mechanics and Engineering*, vol. 200, no. 13, pp. 1343-1353.

Manni, C.; Reali, A.; Speleers, H. (2015): Isogeometric collocation methods with generalized B-splines. *Computers & Mathematics with Applications*, vol. 70, no. 7, pp. 1659-1675.

Mansur, W. J.; Vasconcellos, C. A. B.; Zambrozuski, N. J. M.; Rotunno Filho, O. C. (2009): Numerical solution for the linear transient heat conduction equation using an Explicit Green's Approach. *International Journal of Heat and Mass Transfer*, vol. 52, no. 3-4, pp. 694-701.

Marussig, B.; Zechner, J.; Beer, G.; Fries, T. P. (2015): Fast isogeometric boundary element method based on independent field approximation. *Computer Methods in Applied Mechanics and Engineering*, vol. 284, pp. 458-488.

Natarajan, S.; Wang, J. C.; Song, C.; Birk, C. (2015): Isogeometric analysis enhanced by the scaled boundary finite element method. *Computer Methods in Applied Mechanics and Engineering*, vol. 283, pp. 733-762.

Nguyen, B. H.; Tran, H. D.; Anitescu, C.; Zhuang, X.; Rabczuk, T. (2016): An isogeometric symmetric Galerkin boundary element method for two-dimensional crack problems. *Computer Methods in Applied Mechanics and Engineering*, vol. 306, pp. 252-275.

- Nguyen, M. N.; Bui, T. Q.; Truong, T. T.; Trinh, N. A.; Singh, I. V. et al.** (2016): Enhanced nodal gradient 3D consecutive-interpolation tetrahedral element (CTH4) for heat transfer analysis. *International Journal of Heat and Mass Transfer*, vol. 103, pp. 14-27.
- Nguyen, M. N.; Bui, T. Q.; Yu, T. T.; Hirose, S.** (2014): Isogeometric analysis for unsaturated flow problems. *Computers and Geotechnics*, vol. 62, pp. 257-267.
- Nguyen, V. P.; Kerfriden, P.; Brino, M.; Bordas, S. P. A.; Bonisoli, E.** (2014): Nitsche's method for two and three dimensional NURBS patch coupling. *Computational Mechanics*, vol. 53, no. 6, pp. 1163-1182.
- Qian, X. P.; Sigmund, O.** (2011): Isogeometric shape optimization of photonic crystals via Coons patches. *Computer Methods in Applied Mechanics and Engineering*, vol. 200, no. 25, pp. 2237-2255.
- Peake, M. J.; Trevelyan, J.; Coates, G.** (2013): Extended isogeometric boundary element method (XIBEM) for two-dimensional Helmholtz problems. *Computer Methods in Applied Mechanics and Engineering*, vol. 259, no. 2, pp. 93-102.
- Piegl, L.; Tiller, W.** (1997): *The NURBS Book*, 2nd ed. Springer-Verlag, New York.
- Scott, M. A.; Simpson, R. N.; Evans, J. A.; Lipton, S.; Bordas, S. P. A. et al.** (2013): Isogeometric boundary element analysis using unstructured T-splines. *Computer Methods in Applied Mechanics and Engineering*, vol. 254, no. 2, pp. 197-221.
- Seo, Y.; Kim, H.; Youn, S.** (2010): Isogeometric topology optimization using trimmed spline surfaces. *Computer Methods in Applied Mechanics and Engineering*, vol. 199, no. 49, pp. 3270-3296.
- Shojaee, S.; Valizadeh, N.; Izadpanah, E.; Bui, T. Q.; Vu, T. V.** (2012): Free vibration and buckling analysis of laminated composite plates using the NURBS-based isogeometric finite element method. *Composite Structures*, vol. 94, pp. 677-1693.
- Simpson, R. N.; Bordas, S. P. A.; Lian, H.; Trevelyan, J.** (2013): An isogeometric boundary element method for elastostatic analysis: 2D implementation aspects. *Computers & Structures*, vol. 118, no. 6, pp. 2-12.
- Simpson, R. N.; Bordas, S. P. A.; Trevelyan, J.; Rabczuk, T.** (2012): A two-dimensional isogeometric boundary element method for elastostatic analysis. *Computer Methods in Applied Mechanics and Engineering*, vol. 209-212, no. 324, pp. 87-100.
- Simpson, R. N.; Liu, Z.** (2016): Acceleration of isogeometric boundary element analysis through a black-box fast multipole method. *Engineering Analysis with Boundary Elements*, vol. 66, pp. 168-182.
- Sun, S. H.; Yu, T. T.; Nguyen, T. T.; Atroshchenko, E.; Bui, T. Q.** (2018): Structural shape optimization by IGABEM and particle swarm optimization algorithm. *Engineering Analysis with Boundary Elements*, vol. 88, pp. 26-40.
- Takahashi, T.; Matsumoto, T.** (2012): An application of fast multipole method to isogeometric boundary element method for Laplace equation in two dimensions. *Engineering Analysis with Boundary Elements*, vol. 36, no. 12, pp. 1766-1775.
- Telles, J. C. F.** (1987): A self-adaptive co-ordinate transformation for efficient numerical evaluation of general boundary integrals. *International Journal for Numerical Methods in Engineering*, vol. 24, no. 5, pp. 959-973.

Valizadeh, N.; Bazilevs, Y.; Chen, J. S.; Rabczuk, T. (2015): A coupled IGA-meshfree discretization of arbitrary order of accuracy and without global geometry parameterization. *Computer Methods in Applied Mechanics and Engineering*, vol. 293, pp. 20-37.

Walker, S. P.; Fenner, R. T. (1989): Treatment of corners in BIE analysis of potential problems. *International Journal for Numerical Methods in Engineering*, vol. 28, no. 11, pp. 2569-2581.

Wall, W. A.; Frenzel, M. A.; Cyron, C. (2008): Isogeometric structural shape optimization. *Computer Methods in Applied Mechanics and Engineering*, vol. 197, no. 33, pp. 2976-2988.

Wang, Y.; Benson, D. J.; Nagy, A. P. (2015): A multi-patch nonsingular isogeometric boundary element method using trimmed elements. *Computational Mechanics*, vol. 56, no. 1, pp. 173-191.

Wu, H. T. (2008): *Application of the Boundary Element Methods in Heat Transfer*. National Defense Industry Press, Beijing.

Yao, Z. H.; Wang, H. T. (2010): *The Boundary Element Methods*. Higher Education Press, Beijing.

Yin, S. H.; Yu, T. T.; Bui, T. Q.; Liu, P.; Hirose, S. (2016): Buckling and vibration extended isogeometric analysis of imperfect graded Reissner-Mindlin plates with internal defects using NURBS and level sets. *Computers & Structures*, vol. 177, pp. 23-38.

Yu, B.; Yao, W.; Gao, Q. (2014): A precise integration boundary-element method for solving transient heat conduction problems with variable thermal conductivity. *International Journal of Heat and Mass Transfer*, vol. 78, no. 5, pp. 883-891.

Yu, T. T.; Bui, T. Q.; Yin, S. H.; Doan, D. H.; Wu, C. T. et al. (2016): On the thermal buckling analysis of functionally graded plates with internal defects using extended isogeometric analysis. *Composite Structures*, vol. 136, pp. 684-695.

Yu, T. T.; Yin, S. H.; Bui, T. Q.; Liu, C.; Wattanasakulpong, N. (2017): Buckling isogeometric analysis of functionally graded plates under combined thermal and mechanical loads. *Composite Structures*, vol. 162, pp. 54-69

Zhou, W.; Liu, B.; Wang, Q.; Cheng, Y.; Ma, G. et al. (2017): NURBS-enhanced boundary element method based on independent geometry and field approximation for 2D potential problems. *Engineering Analysis with Boundary Elements*, vol. 83, pp. 158-166.

Appendix A

The main idea of Coons body interpolation method is given. Assume that a domain is surrounded by four boundary curves, i.e., $C(u,0)$, $C(u,1)$, $C(0,v)$, and $C(1,v)$; then the surface $C(u,v)$ in the domain can be interpolated as [Long and Zhang (2017)]:

$$C(u,v) = [1-\alpha(u), \alpha(u)] \begin{bmatrix} C(0,v) \\ C(1,v) \end{bmatrix} + [1-\beta(v), \beta(v)] \begin{bmatrix} C(u,0) \\ C(u,1) \end{bmatrix} - [1-\alpha(u), \alpha(u)] \begin{bmatrix} C(0,0) & C(0,1) \\ C(1,0) & C(1,1) \end{bmatrix} \begin{bmatrix} 1-\beta(v) \\ \beta(v) \end{bmatrix} \tag{A.1}$$

where $\alpha(u)$ and $\beta(v)$ are parameter functions which satisfy the following conditions:

$$\alpha(0) = \beta(0) = 0 \tag{A.2}$$

$$\alpha(1) = \beta(1) = 1 \tag{A.3}$$

With the same interpolation method, we can use the control point on the boundary curves to obtain the internal control points. The control points on the boundary of region are denoted as $\mathbf{P}_{i,j}$ ($i=1,2,\dots,l$, and $j=1,2,\dots,m$), where l is the number of control points in the u direction and m is the number of control points in the v direction. Set $u_0 = (i-1)/(l-1)$, $u_1 = 1-u_0$, $v_0 = (j-1)/(m-1)$, and $v_1 = 1-v_0$; the control points in the domain are obtained with the following interpolation formula:

$$P_{i,j} = [u_1, u_0] \begin{bmatrix} P_{1,j} \\ P_{l,j} \end{bmatrix} + [v_1, v_0] \begin{bmatrix} P_{i,1} \\ P_{i,m} \end{bmatrix} - [u_1, u_0] \begin{bmatrix} P_{1,1} & P_{1,m} \\ P_{l,1} & P_{l,m} \end{bmatrix} \begin{bmatrix} v_1 \\ v_0 \end{bmatrix} \tag{A.4}$$

Appendix B

For geometry with corners, we put two overlap points with the same temperature but different heat conductions of both sides on the corner. If the temperature at corner is known, but the heat conductions on both sides of the corner are unknown, we can first calculate the heat conduction on one side, and then calculate the other side. The formula for calculating the heat conduction at corner is as follows [Walker and Fenner (1989)]:

$$q_u = \frac{1}{\sin \theta} (T'_u \cos \theta - T'_v) \tag{B.1}$$

$$q_v = \frac{1}{\sin \theta} (T'_u - T'_v \cos \theta) \tag{B.2}$$

where T'_u and T'_v are lengthwise gradient vectors which can be calculated with boundary temperature, q_u and q_v are normal gradient vectors shown in Fig. B1.

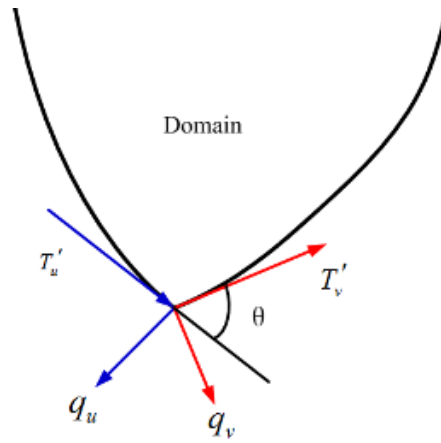


Figure B1: Lengthwise and normal gradient vector at a corner